Performance Evaluation of Signal Processing Tools Used for Fault Detection of Hydro-generators Operating in Noisy Environments

Hossein Ehya, *Student Member, IEEE,* and Arne Nysveen, *Senior Member, IEEE*

***Abstract*—Signal Processing plays a crucial role in addressing failures in electrical machines. Experimental data are never perfect due to the intrusion of undesirable fluctuations unrelated to the investigated phenomenon, namely so-called noise. Noise has disturbing effects on the measurement data and, in the same way, could diminish or mask the fault patterns in feature extraction using different signal processors. This paper introduces various type of noise occurring in an industrial environment. Several measurements are performed in the laboratory and power plants to identify the dominant type of noise. Fault detection in a custom made 100 kVA synchronous generator under an inter-turn short circuit fault is also studied using measurements of the air gap magnetic field. Signal processing tools like a fast Fourier transform (FFT), short-time Fourier transforms (STFT), discrete wavelet transforms (DWT), continuous wavelet transforms (CWT), and time-series data mining (TSDM) are used to diagnose the faults, with a central focus on additive noise impacts on processed data. Two novel patterns are introduced based on STFT and CWT for inter-turn short circuit fault detection of synchronous generators that do not need a priori knowledge of a healthy machine. Useful methods are presented for hardware noise rejection.**

***Index Terms*—Fault diagnosis, inter-turn short circuit, noise rejection, salient pole synchronous generator, short-time Fourier transforms, signal processing, time-domain analysis, wavelet transforms.**

I. Introduction

EARLY stage diagnosis of incipient faults in electrical machines can limit the progressive damage that leads to substantial economic losses. Over the past two decades, sustained research activity has been conducted in the field of fault detection of electrical machines. Faults in hydro-generators are divided into two categories: electrical faults, such as short circuit faults of stator windings or inter-turn short circuit (ITSC) faults in rotor field windings, and mechanical faults, such as static or dynamic eccentricity, broken damper bars, broken end rings, and misalignment. Each type of fault in an electrical machine can give rise to a specific symptom, which may be observed in a measured signal [1].

The working environment of electrical machines in the industries and power plants is susceptible to various kinds of noise that may have considerable consequences on the measured signals [2] The working environment of synchronous generators in hydropower plants is vulnerable to noise emitted from power transformers, power station bus-bars and switch-gear, the turbine, and the machine itself. In addition, industrial induction motors controlled by a static converter may create interfering noise [3]–[5]. The amplitude and frequency of the emitted noise by the converter depend on the modulation techniques used in the power converter [6].

Previous studies [7] have shown that the majority of industries are subjected to a high degree of complex noise, which is the combination of white Gaussian noise and impulsive noise. The amplitude of the noise in the working environment of the industry depends on various criteria [8] and the noise profile varies from case to case. In addition to noise emitted from the equipment used in the industry, faulty electrical machines also cause some degree of noise [9], and the noise level is increased with the increasing severity of the fault.

Feature extraction and signal processing is the central part of a fault detection procedure. Numerous indices are proposed based on the various signal processing tools capable of detecting different types of faults in electrical machines. The main component of fault detection is a measured signal from the faulty machine in the form of an air-gap magnetic field, stator or rotor current, voltage, stray magnetic field, or torque. If the working environment is vulnerable to noise, having a signal not contaminated by noise is almost impossible, indicating that the noise effect on the measured signal must be considered. In addition, the noise might affect the fault signature extracted by signal processing tools and result in a false alarm, since various signal processing tools might respond differently to the noise presence.

Fast Fourier transforms (FFT) is the most commonly applied signal processing tool in the fault detection of electrical machines. The FFT is applied to the stator current and the voltage, torque, air gap magnetic field, and stray magnetic flux of different electrical machines, such as induction motors, permanent magnetic machines, and salient pole synchronous machines, to detect a fault [1], [10]–[14]. Although FFT is simple and has low computational complexity, it does not show clear changes in the spectrum plot for a fault with low severity nor does it determine the type of fault. Moreover, FFT only depicts the frequency contents of the signal, whereas it lacks time representation. Therefore, the demand for methods that could overcome these shortcomings has resulted in advanced signal processing tools, such as short-time Fourier transforms (STFT), continuous wavelet transforms (CWT), and discrete

This work was supported by the Norwegian Research Centre for Hydropower Technology (HydroCen) partly funded by The Research Council of Norway (contract no. 257588).

Hossein Ehya, and Arne Nysveen are with Department of Electrical Power Engineering, Norwegian University of Science and Technology, Trondheim, 7491, Norway. (corresponding author phone: +47 47743322; e-mail: hossein.ehya@ntnu.no).

wavelet transforms (DWT).

Application of these advanced signal processing tools to fault detection problems has indicated that they could meticulously identify a certain pattern due to the specific type of fault in electrical machines. For instance, STFT is used to detect broken bars and inter-turn short circuit faults in salient pole synchronous generators [15]–[17] and was able to provide a unique pattern for each type of fault. In [18], [19], CWT was used to identify broken bars and eccentricity faults in induction motors. Unlike STFT and CWT, which provide a qualitative representation of a measured signal, DWT classifies the signal into different frequency bands. DWT has been used to diagnose different kinds of faults in induction motors [18], [19], salient pole synchronous generators [20], and permanent magnet machines [21]. These advanced signal processing tools have been widely used for fault detection in electrical machines, but they have not considered the noise effect, although some attempts have been made to address this issue in [22].

The present work is a detailed study of the noise impact on the signal processing tools used in the fault diagnosis of hydroelectric synchronous generators and how noise impact must be considered in the fault detection procedure as depicted in Fig. 1. The Hall-effect sensor is used to measure the air-gap magnetic field since it is exposed to both internal noise generated by the machine and external noise in the environment. A custom-made 100 kVA synchronous generator is used to conduct the ITSC fault and provide the required data. Section II presents a definition of signal and noise. It also thoroughly presents a source of noise in a power plant and industry. Various types of noise are introduced to provide a perspective for characterizing the existing types of noise in a power plant. In section III, the experimental setup used to measure the air-gap magnetic field is explained. The results of two field tests are discussed to show the existence of noise in the hydropower plants. In section IV, the effects of noise on signal processing tools, such as FFT, STFT, CWT, DWT, and time-series data mining (TSDM), are investigated. The impacts of noise on the extracted signature by the signal processing tools are discussed. The obtained results demonstrate how a certain level of noise can deteriorate the fault signatures.

II. SIGNAL AND NOISE

A. Definition

The term ‘signal’ in the field of condition monitoring means only that desirable data that are measured. However, signals are vulnerable to noise during the process of acquisition, storage, or conversion. Noise is an unwanted signal that may disrupt the quality of the main signal. Every device in the power plant or industry that works based on electromagnetic law may act as a noise source. The noise generated by each electric device has its own unique characteristics that fall into a specific category of noise. The noise level can be expressed as a ratio of the power in one Hertz of bandwidth (dBm/Hz), where power is expressed in units of (dBm). The quality of the signal is quantified by expression of the signal-to-noise ratio. It represents the ratio of the signal amplitude to the standard deviation of the noise [2].

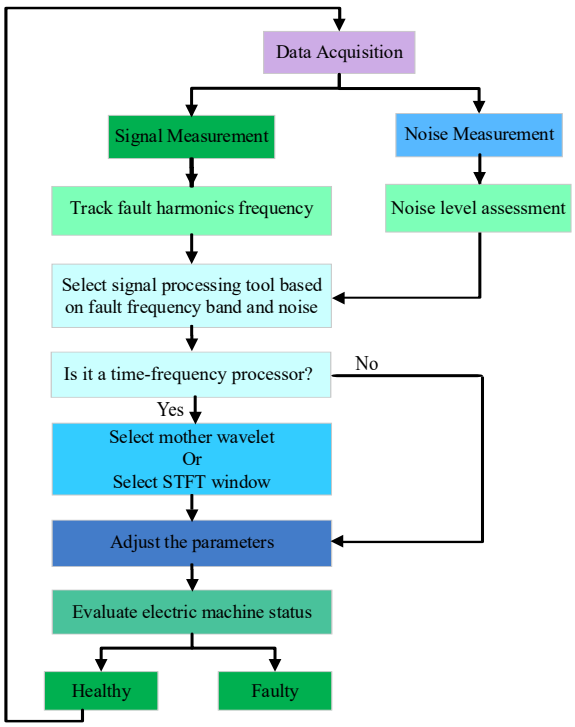

Fig. 1. The flowchart for fault detection.

B. Source of Noise in Industries

The noise radiated from electric equipment is generally limited to a discrete low-frequency signal. However, an electrical machine, whether stationary (e.g., transformers) or rotating (e.g., electric motors or generators), generates a broadband noise component due to their cooling systems. The net noise is superimposed on the electromagnetic and cooling system components. The noise in an electric machine can be represented as below [2], [5]:

1) The magnetic source of noise in the electrical machine is due to the radial force created by the interaction of the stator and rotor magnetic field. When magnetic flux inside the air-gap passes in a radial direction, a radial component of the force creates a vibration and noise. A severe resonance happens if a frequency of the radial force components coincides with a natural frequency of the machine. Acoustic noise is one of the consequences of the resonance in the machine. The structure of the rotor and the slot harmonics cause high-frequency components that, in turn, lead to force and noise inside the machine. Moreover, there exist some other sources of magnetic noise including a product of the space harmonics of stator and rotor winding, a product of space harmonics of the stator winding and the eccentricity fault, and the product of stator space harmonics and the rotor saturation harmonics.
2) The aerodynamic source of noise has a broad frequency band (100 Hz – 10 kHz) that is generated due to the flow of the air at the inlet or outlet of the machine cooling system. The fans either inside the machine driven by the shaft or the external can generate acoustic noise. The

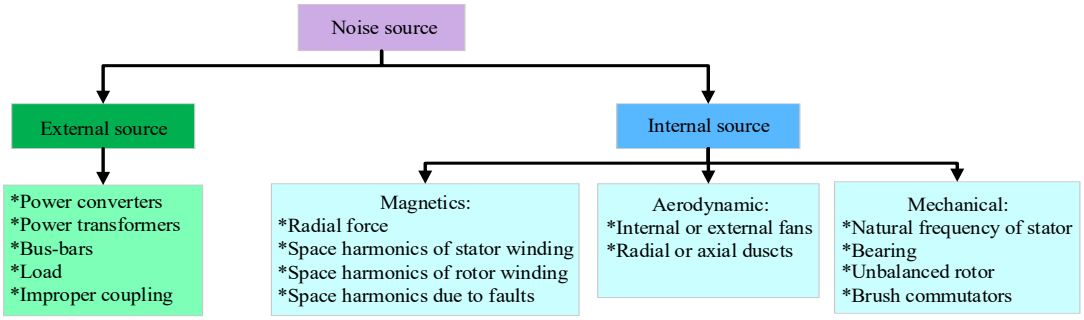

Fig. 2. Sources of noise in the industries and power plants.

axial or radial ventilation ducts inside the stator core also contribute to the noise.

3) The mechanical source of noise arises due to the natural frequency of the stator, improper installation of the machine, shaft and bearing vibration. If the exciting frequency of the machine coincides with the stator's natural frequency, a strong noise will be created. The improper coupling between the shaft of the synchronous machine and the driving component or the load is also accounted as a mechanical source of the noise. There exist three main factors that result in a mechanical noise due to bearings, brush commutators, and the unbalanced rotor during manufacturing. The sleeve bearing compared with the rolling bearing contributes to less noise, however, the rolling bearing is preferred due to low cost especially in low-power electric machines.

The amount of noise created by transformers is significant in comparison to the noise in rotating electrical machines. The source of the noise in power transformers is divided into magnetic noise, which is due to the magnetic field of the core, and the load noise, which is caused due to interaction of the leakage flux and the current passes through the coils [3]. However, the metallic body of the transformer may shield the emitted noise from the working environment, even if the generated noise is unavoidable. The power transformers in power plants are also placed in a separate room for safety reasons, and this further reduces their effect on the measured signal from the synchronous generator. Bus-bars that carry large current from the generator to the transformer are another source of noise in power plants.

Many electrical motors use solid-state converter drives to feed power sources into the windings. The power supply is not entirely sinusoidal and contains numerous harmonics and sub-harmonics. The most important harmonics created are 5^{th}, 7^{th}, and 11^{th}, which become critical if these harmonics coincide with a natural frequency of the stator [4]. The net forces due to the power electronics harmonic components result in significant noise. Figure. 2 shows the different sources of noise.

C. Various Types of Noise

Various types of noise, based on their properties, have different effects on the measured signal. The signal from the noise can be discriminated based on the frequency components.

TABLE I
100 kVA, 50 Hz, SYNCHRONOUS GENERATOR TOPOLOGY SPECIFICATION AND NAMEPLATE DATA

Quantity	*Values*	*Quantity*	*Values*
Winding connection	Wye	Number of poles	14
No. of stator turns	8	No. of rotor turns / pole	35
Nominal speed	428 rpm	Power factor	0.90
Nominal voltage	400 V	Nominal current	144.3 A
Nominal exc. current	103 A	No-load exc. current	53.2 A

The signal may contain mostly low-frequency components, whereas the noise may spread out over the wide frequency range or the noise may only contain high-frequency components. The noise is characterized based on its frequency spectrum, which is commonly described in terms of noise color. The noise is categorized as white noise, pink noise, Brownian noise, blue noise, and violet noise. Each type of noise is specified according to the frequency distribution of its power spectral density, as shown in Fig. 3.

1) White noise is a random noise that has equal power over the entire frequency range.
2) Pink noise is characterized by high power at low frequencies, and its power is diminished by increasing the frequency.
3) Brownian noise's amplitude is proportional to the square of the frequency over a frequency range.
4) Blue noise has strong power at high frequency and is not common in experimental measurements.
5) Violet noise, which is a differentiation of white noise, has a power spectral density that is proportional to the square of the frequency over the finite range.

III. LABORATORY AND FIELD TESTS

A. Experimental Setup

Fig. 4 shows the experimental setup used in this paper with a detailed specification as shown in Table. I. A custom-made 100 kVA, 400 V, synchronous generator with 14 salient poles is used to investigate the noise effect on an air-gap magnetic field signal under an ITSC fault. A 90 kW, 4 pole induction motor is used to rotate the coupled synchronous generator. The induction motor shaft is connected to the generator by a gearbox with a gear ratio of $1/3$. A programmable converter is used to feed the induction motor. The field winding of the generator is supplied by a DC power supply. A copper plate is

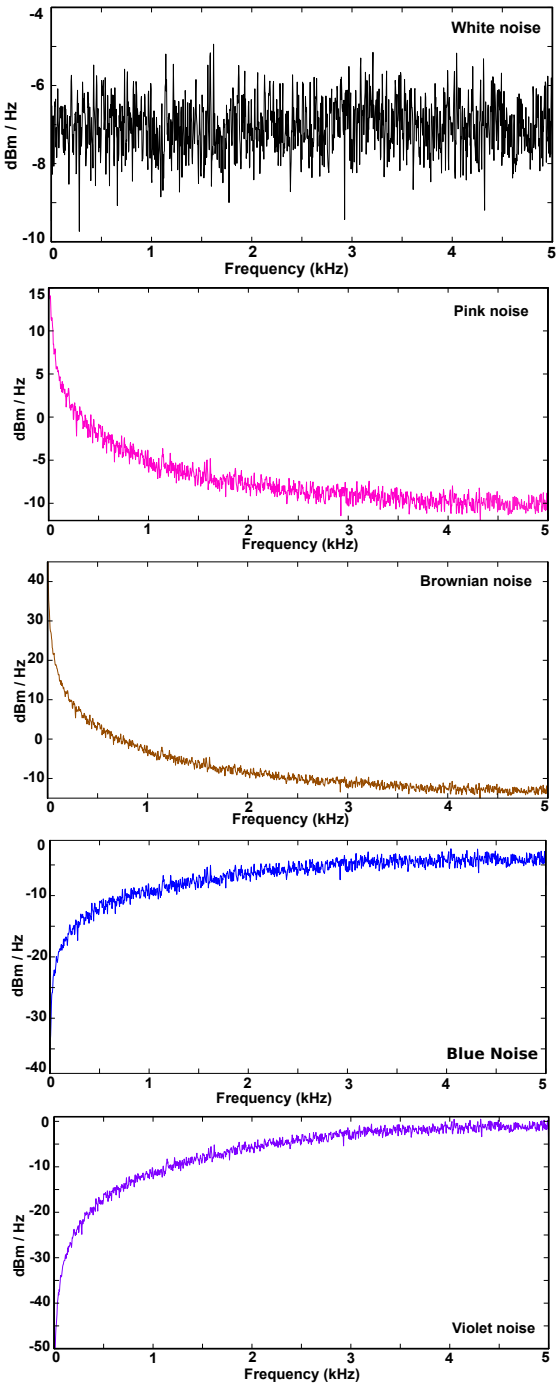

Fig. 3. The prevalent type of noise based on their color definition. White Gaussian noise, Pink noise, Brownian noise, Blue noise, Violet noise.

used to create the ITSC fault on one of the rotor field windings, as shown in Fig. 4. A Hall-effect sensor (AST244), with a ratio of the induced voltage to the magnetic field equal to 2.54 T/V, is installed on the stator tooth to acquire the air gap magnetic field (Fig. 4). The data sheet specifies that the sensor should be supplied by a 2 mA DC current source. However, due to considerable electromagnetic interference, the magnitude of the current power supply is increased to 4 mA to increase the signal-to-noise ratio (SNR). A high-resolution (16-bit) oscilloscope is used to sample the data at 10 kHz.

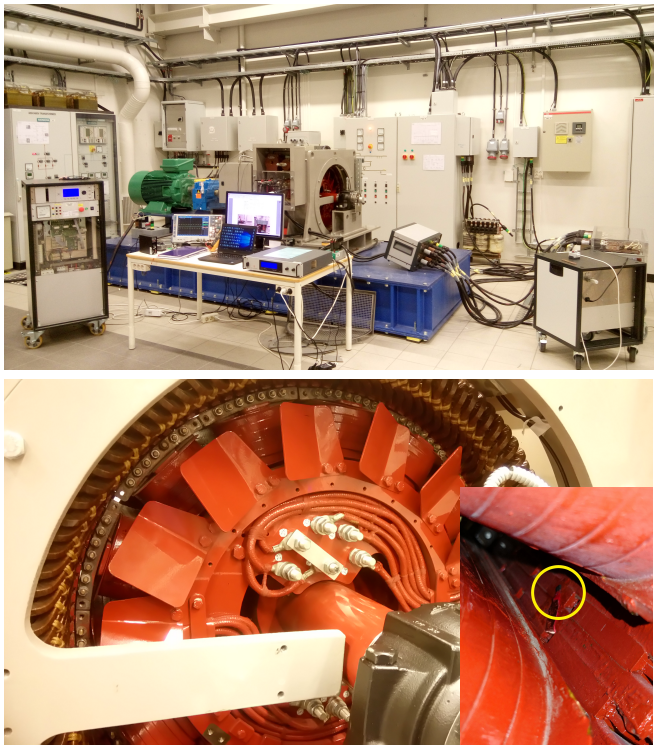

Fig. 4. The laboratory setup of a 100 kVA salient pole synchronous generator (top). The copper plate used to apply the ITSC fault on one of the rotor field windings, the installed Hall-effect sensor on the stator tooth of a laboratory setup (bottom).

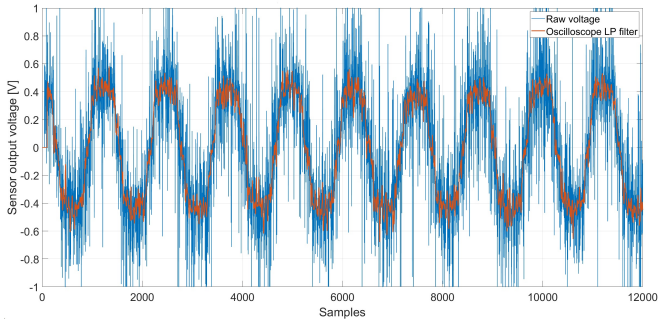

Fig. 5. The measured air gap magnetic field of the synchronous generator in the laboratory in the presence of a significant noise impact (blue waveform) and the applied low-pass filter of the oscilloscope to diminish the noise impact (red waveform).

The test procedure for the experimental setup is as follows: tests were conducted in both a healthy state and under the ITSC fault at different degrees of severity. The synchronous generator is accelerated using an induction motor until it reaches its nominal speed. The nominal magnetizing current is applied to the rotor field winding to achieve a nominal voltage in the stator terminals. The ITSC fault is conducted at a standstill by removing the desired number of turns from the rotor field winding using a copper plate. Fig. 5 represents the measured air gap magnetic field in the presence of noise. The signal is analyzed to recognize the type of noise that leaked into the signal. The separated power spectrum of the noise from the measured air-gap magnetic field shows that its behavior resembles that of white Gaussian noise.

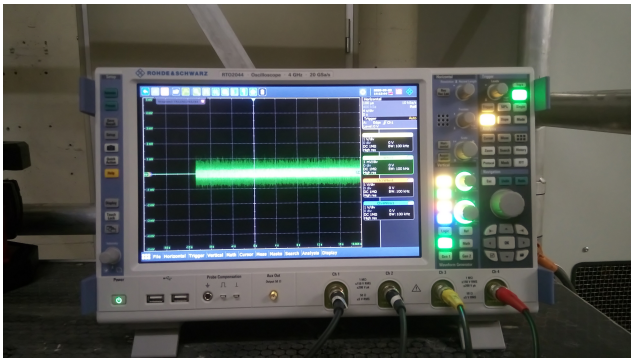

Fig. 6. Measured noise in hydropower plant.

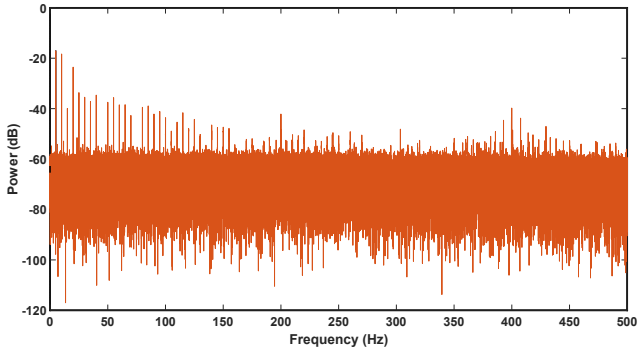

Fig. 7. Spectrum density of a measured noise in a hydropower plant.

B. Field Tests

Field tests were conducted in two power plants: a power plant with a single unit generator and another power plant with four units. Hall-effect sensors were installed on the stator tooth, and the data were measured while the generator was at standstill. Therefore, the measured data, as shown in Fig. 6, represent the noise in the working environment of the hydro-generator. The power spectrum of a measured noise is depicted in Fig. 7, which indicates that a white Gaussian noise exists with a 70 dB SNR. The measured noise for a power plant with only one unit shows a lower SNR, thereby showing the impact of electric power equipment on the generated level of noise.

IV. Signal Processing

Signal processing is a core part of the fault detection procedure. Although the measured signals from the electrical machines, whether in a healthy or faulty state, contain useful data, they must be analyzed using signal processing tools. The signal processing tools are categorized into the following three domains:

1) Time-domain
2) Frequency domain
3) Time-Frequency domain

Several methods are available, based on time, frequency, and time-frequency domains. In this paper, TSDM is used as a time-domain processor. The FFT, which is a frequency domain processor, is used to obtain the frequency spectrum density of the signal. The wide range of time-frequency processors is limited in this paper to STFT, CWT, and DWT.

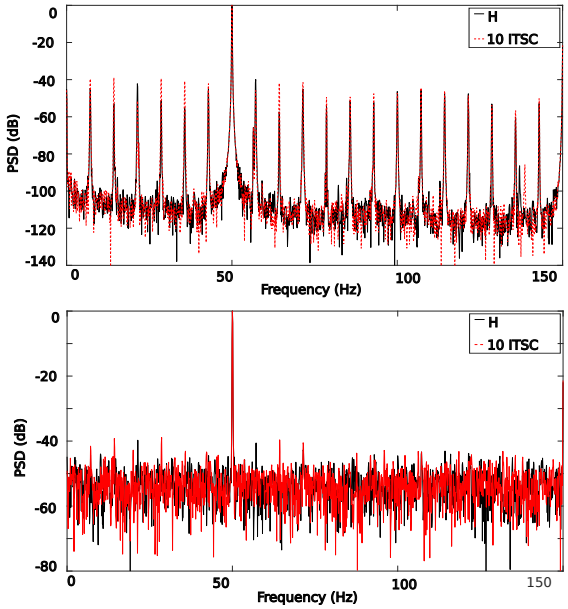

Fig. 8. The spectrum density of an air gap magnetic field in a healthy state and under a 10 ITSC fault, a) without noise interference (top), b) with 20 dB SNR (bottom)

A. Fast Fourier Transform

The Fourier transform represents the desired function as its constituent harmonic components and the Fourier transform is a convolution operation. A Fourier series is a periodic function and it requires that the processed signal must be periodic. Since the majority of the measured time series are not periodic, it assumes that the entire measured data series is one periodic function. A discrete Fourier transform is formulated for a discrete signal that represents the frequency contents of the time data series and the fast Fourier transform is a commonly applied approach to achieve a discrete Fourier transforms [23]. FFT is computationally efficient and it reduced the computational complexity of discrete Fourier transform from $O(m^2)$ to $O(mlog(m))$, where m is the total number of samples. The spectral representation of the time signal consists of periodic components in the frequency domain that each has a specific frequency, phase angle, and amplitude. The FFT can provide a general representation of the frequency contents of the signal. The amplitude of the frequency spectrum is increased if a signal changes. Indicating that FFT can track the faulty signal variation in the frequency spectrum, but the provided information based on frequency spectrum is not informative unless the fault frequency is known. Moreover, the accuracy and precision of the spectrum density of the signal depends on the number of sampled data and the sampling frequency of the signal.

The distorted magnetic field caused by an ITSC fault contains sub-harmonics that can be distinguished using FFT based on the following features:

$$f_{sub-harmonic} = \frac{(p \pm k) f_s}{p} \tag{1}$$

where f_s is the stator terminal frequency, p is the number of poles, and k is an integer. Fig. 8. depicts the spectral density

TABLE II
THE EFFECT OF VARIOUS SIGNAL-TO-NOISE RATIOS ON THE NOMINATED SIGNATURE IN A HEALTHY STATE AND UNDER AN ITSC FAULT (GRAY COLORS)

Noise Level	*7.15 Hz*	*14.3 Hz*	*28.6 Hz*	*35.7 Hz*	*64.3 Hz*
No-Noise	-44.6	-53.1	-51.3	-54.9	-57.4
60 dB	-44.6	-52.9	-51.2	-55.0	-57.6
50 dB	-44.8	-53.1	-51.4	-54.1	-57.8
40 dB	-45.1	-53.0	-51.1	-55.3	-58.2
30 dB	-45.3	-55.1	-51.5	-54.8	-57.3
No-Noise	-39.6	-38.9	-39.4	-40.8	-41.8
60 dB	-39.6	-38.9	-39.4	-40.8	-41.8
50 dB	-39.5	-38.9	-39.4	-40.8	-41.9
40 dB	-39.8	-39.1	-39.2	-40.6	-42.1
30 dB	-40.3	-39.1	-39.9	-40.2	-41.8

of the air gap magnetic field in the healthy state and under a 10 ITSC fault in one of the rotor poles, as obtained by the FFT processor. Increasing the number of shorted turns in the rotor field winding also increases the amplitude of the side-band components. For instance, the amplitude of the side-bands for a 10 ITSC fault at frequency 7.15 Hz, 14.3 Hz, 28.6 Hz, and 35.7 Hz increased from -44.6 dB, -53.1 dB, -51.3 dB, and 54.9 dB to -36.6 dB, -38.9 dB, -39.4 dB, and -40.8 dB, respectively.

Fig. 8 demonstrates the effect of 20 dB white Gaussian noise on the spectral density of the air-gap magnetic field in a healthy state and under a 10 ITSC fault. The noise level of the frequency spectrum is increased from -100 dB to -50 dB by decreasing the SNR. Therefore, the magnitude of the introduced feature for ITSC detection is simply masked in the case of high-level noise interference. Hence, the ITSC diagnosis under a 30 dB SNR is almost impossible.

Table II presents the effect of various SNRs on the nominated feature under an ITSC fault. The amplitude of the index for a low degree of SNR is acceptable, since the ITSC fault can be identified. However, the SNR of 20 dB is the borderline for accurate fault detection. By decreasing the SNR, the amplitudes of the side-bands in both the healthy and faulty cases are masked and the faulty side-band components cannot be identified. The side-band component of the healthy case is also increased and its amplitude is similar to that of a faulty case without noise impact and may result in a false alarm indication of a fault.

B. Short-Time Fourier Transform

The STFT performs a time-frequency analysis that represents both the frequency and time contents of a signal. STFT uses a fixed basis function, like FFT. In addition, the signal transformation is performed by sweeping a fixed window function over a signal. STFT, compared with FFT, provides a better temporal and frequency localization. However, according to the uncertainty principle, the product of temporal and frequency resolution is constant; therefore, achieving an acceptable time and frequency resolution at the same time is impossible. Moreover, STFT has a superiority over the FFT since it can analyze the non-stationary signals. The mathematical representation of the STFT is shown as below:

$$STFT(f,t) = \frac{1}{2\pi}\int_{-\infty}^{\infty} x(t)h(t-\tau)e^{-i2\pi f\tau}d\tau \qquad (2)$$

where h(t) is the window function. There exists numerous type of window function which must be selected according to the signal characteristics for optimal result. The end effect must be considered since it may result in a false decision of fault and it can be mitigated using a proper window function including, flat top, Nuttall, Dirichlet, Bartlett-Hann, Parzen, Blackman, Blackman-Harris, Chebwin, exponential, triangular, Hamming, Hann, Gaussian, Bartlett, Bohman, Kaiser, and Slepian. There exists not a straightforward rule to find an appropriate window function, indicating that several window functions must be performed. The length of the data in addition to the window length are also the main factors that must be considered during parameter adjustment. The time resolution of the STFT is inversely proportional to the length of the time window while the frequency resolution of the STFT has a direct relationship with the length of the window function. The computational complexity of the STFT compared with FFT is negligible since the computational complexity of the STFT is $O(n.mlog(m))$ where n is window length. Indicating that the FFT is performed n times. The percentage of the window overlapping when the window function sweeps across the data is a key point since window overlap can give a more analysis point and higher resolution across time, but the computational cost becomes higher. Therefore, a trade-off must settle down to have adequate analysis points to achieve a smooth result across time while the computational cost does not increase significantly.

Nevertheless, STFT is widely used in feature extraction for fault detection of electrical machines. Fig. 9 and Fig. 10 present the application of STFT to the measured air gap magnetic field in a healthy state and a 10 ITSC fault without a noise effect and with white additive Gaussian noise with SNR of 40 dB and 20 dB. The STFT is performed with a window length of one electric period. A novel index using STFT is introduced that does not require a priori knowledge of the healthy machine. A comparison between the healthy and faulty STFT reveals that the fault has a significant impact on a frequency band of STFT between 50 Hz and 75 Hz. In a case of a healthy machine, there is a uniform pattern with the same intensity pattern along with the mentioned frequency band. Having a 10 ITSC fault in one of the rotor field winding results in a clear periodic intensity reduction in a frequency band between 50 Hz and 75 Hz. The width of a red window in an STFT plot is equal to 140 ms, which represents one mechanical revolution of the synchronous generator, and the widths of a faulty pole are equal to 10 ms which is shown with a blue window. The blue window with a reduced intensity is periodic which shows a faulty pole in the time-frequency plot. Conclusively, the frequency pattern of the desired frequency band in a healthy operation is uniform while having a fault result in a periodic window with widths equal to a rotor pole.

The demonstration that STFT applied to an air-gap magnetic field signal interfered with a 40 dB SNR in healthy and faulty cases shows that detection of the fault is possible, since noise

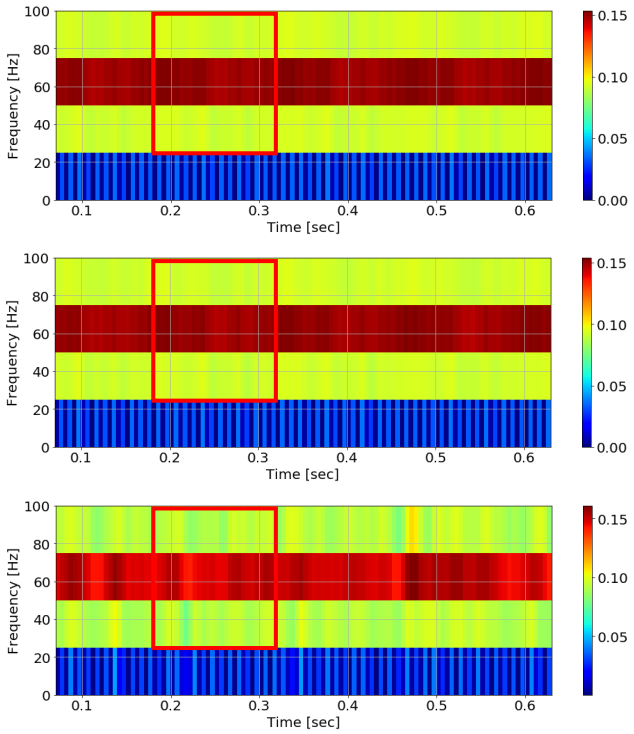

Fig. 9. The applied STFT to an air gap magnetic field in healthy case, without noise impact (first row), 40 dB SNR (second row), and 20 dB SNR (third row)

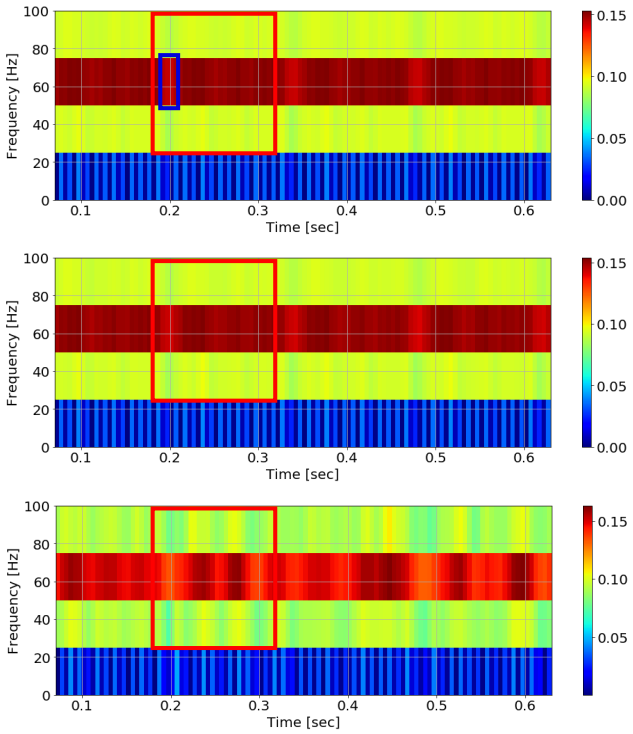

Fig. 10. The applied STFT to an air gap magnetic field under a 10 ITSC fault, without noise impact (first row), 40 dB SNR (second row), and 20 dB SNR (third row)

does not change the available pattern. By contrast, the STFT plot of the signal with 20 dB white Gaussian noise disturbs the fault pattern and fault detection is not possible. A qualitative comparison of the healthy and faulty signal by the introduction of noise implies that noise does not mask the frequency band and fault feature to a great extent up to 40 dB of noise, and this likely reflects the long window length. Therefore, noise with a higher ratio may lead to false fault identification. A caveat of STFT analysis in the presence of noise is that increasing the window length to reject noise will reduce the temporal resolution and limit its usefulness.

C. Continuous Wavelet Transform

Wavelet transform is a signal processing method that decomposes a signal into a set of primary waveforms that, by analyzing the wavelet coefficients of waveforms, may provide some insight. Wavelet transform tries to alleviate the constraints of STFT by defining a mother wavelet as a basis function. Wavelet transform includes numerous mother wavelets, unlike STFT that has a single basis function. Wavelet transform divides a time-frequency space from coarse to fine sizes, while STFT divides a time-frequency space into equal sizes. Moreover, the transform convolutes the signal to the mother wavelet while in STFT the window function is dilated over the entire time series to perform the FFT [24].

Different frequencies in the signal can be tracked by compressing or stretching the wavelet using the wavelet scaling factor. The convolution computation is applied as (3) to the signal and the obtained result is depicted in the time-frequency plot.

$$X(a,b) = \frac{1}{\sqrt{a}} \int_{-\infty}^{\infty} x(t) \Psi^* \left(\frac{t-b}{a} \right) dt \tag{3}$$

The analyzed signal is denoted by $x(t)$ and the Ψ represents the mother wavelet. The scaling factor and the temporal center of the wavelet are adjusted by a and b. The type of mother wavelet must be chosen depends on the type of signal, the frequency of interests, and the investigated properties in the signal. Indicating that there exists no clear rule of thumb to select the mother wavelet and it must be selected by try and error. However, a general rule indicates that a mother wavelet must be used that is similar to the measured signal. For instance, a Haar wavelet can be utilized if the signal has a sudden transition while a Morelet mother wavelet is suitable when the signal has a smooth variation [25]. The computational complexity of the CWT is $(O(m))$ where m is the length of data. A comparison between the computational complexity of the CWT and FFT indicates that FFT performs slower than CWT. Conclusively, the CWT also outperforms faster than STFT since the computational complexity of the STFT is n times the computational complexity of the FFT. The data interpretation of the processed signal by CWT is arduous since it must be analyzed by a convolutional neural network or image processing expert which make its application difficult.

The CWT is a qualitative signal processing tool that is widely used in fault detection of electrical machines [13]. A novel index using the frequency B-spline mother wavelet is introduced to diagnose the ITSC in the rotor field winding based on CWT. Finding healthy state data of a synchronous generator that operates for decades in a power plant is almost

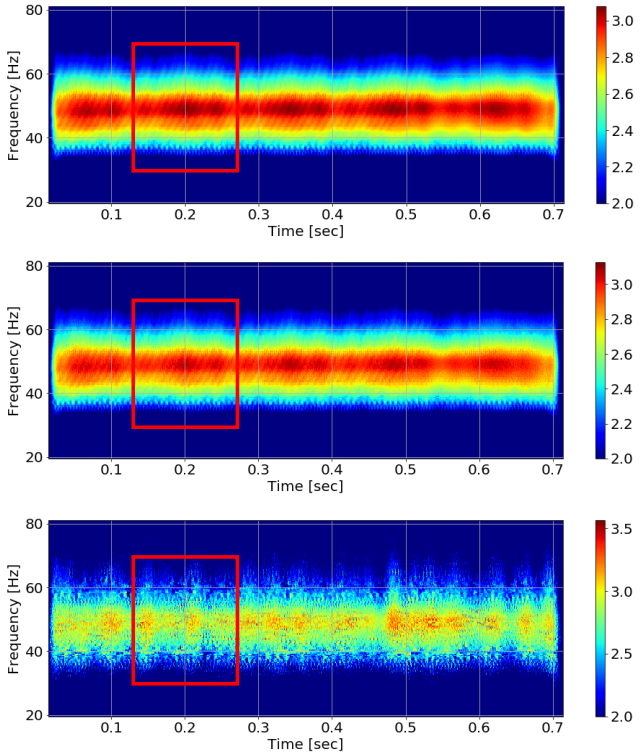

Fig. 11. The applied CWT to an air-gap magnetic field in healthy case in no-noise (first row), 40 dB SNR (second row), and 20 dB SNR (third row).

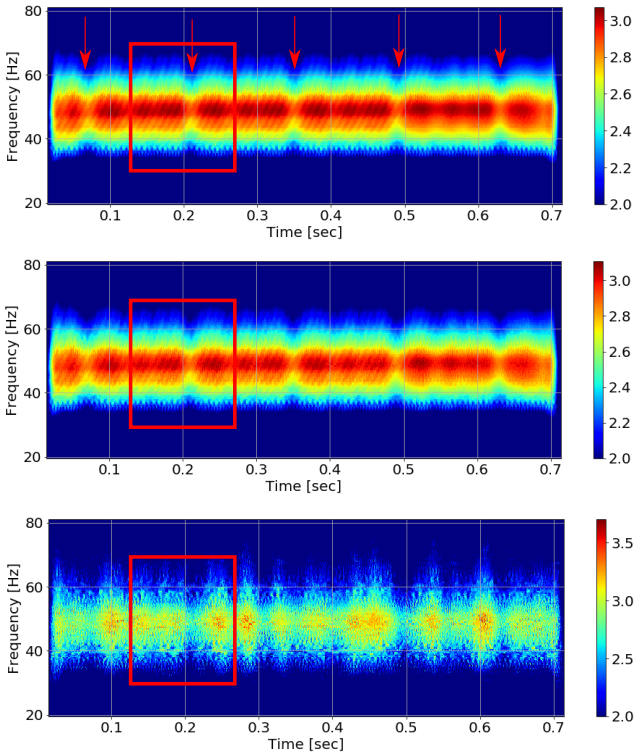

Fig. 12. The applied CWT to an air-gap magnetic field in a 10 ITSC fault case in no-noise (first row), 40 dB SNR (second row), and 20 dB SNR (third row).

impossible. Indicating that a method that can independently indicate the health status of the generator is required. Application of fault detection algorithm based on CWT to the air-gap magnetic field as shown in Fig. 11 generate a uniform frequency band with a various intensity map. Having a short circuit fault in the rotor field winding result is an appearance of a periodic notch in the time-frequency plot. A periodic notch pattern repeated when a faulty pole passes over the installed sensor in the air-gap. Fig. 11 and Fig. 12 depict the application of CWT to a measured air gap magnetic fields of a healthy and faulty machine. A comparison between the healthy state and a 10 ITSC fault between the frequency bands of 40 Hz to 60 Hz indicates that the presence of a fault changes the CWT profile by introducing a periodic notch.

The effect of white Gaussian noise on CWT is studied by adding different amounts of noise. Fig. 11 and Fig. 12 show the impact of 40 dB and 20 dB noise on CWT plots in both healthy and faulty cases. A signal with a SNR up to 40 dB noise does not show significant changes and identifying the changes due to ITSC fault is still possible, while the intensity of the CWT is reduced by decreasing SNR level. Moreover, a signal with SNR equal to 20 dB completely destroys the shape of pattern in both healthy and under ITSC fault. The CWT is affected uniformly across frequencies, unlike the STFT, due to its greater time-frequency resolution. This effect will vary among wavelets. Some of the noise-rejecting qualities of STFT could be achieved in CWT by selecting wavelets with a greater number of oscillations, such as the Shannon mother wavelet.

D. Discrete Wavelet Transform

The DWT is based on the same principle as the CWT since the DWT is commonly implemented based on filter banks. Each level of the filter consists of a low-pass filter and a high-pass filter in which the output is down-sampled by a factor of 2 at each level. The output of the high-pass filter plus the downsampling is known as a detailed signal (h(n)), while the output of the low-pass filter plus downsampling is called an approximate signal (g(n)). The output of the detail coefficient is saved while the output of the approximate coefficient is fed to the next level of the DWT. This process continues until the desired number of decomposition is achieved. Fig. 13 shows one level of the DWT.

The decomposed signal by DWT depends on the type of selected mother wavelet. Daubechies wavelet and Haar wavelet are two commonly applied mother wavelet in DWT. The computational complexity of the DWT is similar to CWT while in practice it is faster than CWT since the data are downsampled in each level. A better temporal resolution can be achieved by CWT compared with DWT since it can shift the filter only by one sample, but higher storage is required in CWT. A frequency tracking of the DWT compared with CWT and STFT is simpler since the mother wavelets are limited. The frequency of interest must be determined and based on that the number of DWT levels must be picked out, if not the frequency of interest appears in two different detail sub-bands. In this paper, Daubechies 8 is used to decompose the air gap magnetic field into various frequency sub-bands. Since the sampling frequency is 10 kHz, the first and second

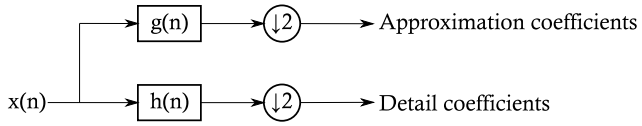

Fig. 13. One level DWT including the filtering and the downsampling procedures.

detailed sub-band are between 5000-2500 Hz and 2500-1250 Hz, respectively.

The discrete wavelet transform is a useful signal processing tool for feature extraction of an electrical machine under a faulty condition. Various features can be extracted from detail sub-bands of DWT such as standard deviation, median, mean, entropy, skewness, kurtosis, variance, and various energies. In this paper, the energy of each sub-band level is introduced as a proper signature to diagnose the occurrence of the ITSC fault. The energy of the signal is as follows:

$$E = \int_{-\infty}^{\infty} |D_n|^2 dt \tag{4}$$

where D_n is the magnitude of each DWT sub-bands. The occurrence of a 10 ITSC fault in one of rotor poles leads to an increment of the energy of D1 to D6 from 1.35, 1.06, 1, 0.97, 0.94, and 0.83 to 0.65, 0.72, 0.79, 0.83, 0.88, and 0.81, respectively. A comparison between the energy variation of the different wavelet sub-bands in a healthy and faulty case provides an accurate indication of the occurrence of an ITSC fault.

Having an air-gap magnetic field signal with a SNR up to 40 dB does not disturb the introduced feature, whereas the signal with a SNR equal to 20 dB changes the results significantly. Fig. 14 shows the discrete wavelet transforms of the air-gap magnetic field in a healthy case without a white Gaussian noise effect and under a noisy condition with a 20 dB SNR. As shown in Fig. 14, the 20 dB noise significantly changes the amplitude and shape of some of the sub-bands, like D5, D4, D3, D2, and D1 even in a healthy case, while it does not change the sub-bands level of D6, D7, and D8. However, the energy of wavelet sub-bands of the healthy generator with 20 dB white Gaussian noise is equal to the energy level of the corresponding wavelet sub-bands under a 10 ITSC fault. For instance, the amplitude of the energy of the sub-bands of D3, D2, and D1 for the healthy generator with 20 dB SNR is decreased to 0.79, 0.72, and 0.65, while the energy of the same sub-bands for a 10 ITSC fault is also the same. Consequently, the noisy environment leads to a false alarm of a fault occurrence in a healthy generator. Table III shows the result of DWT applied to the healthy and faulty generator. The application of DWT for fault detection of the electric machines in a noisy environment must be evaluated based on a sub-band level on which the signature is defined, since some of the low-frequency sub-bands do not undergo any changes even with 20 dB noise.

E. Time Series Data Mining

TSDM is a time-domain nonlinear signal processing tool that is developed based on discrete stochastic models of the

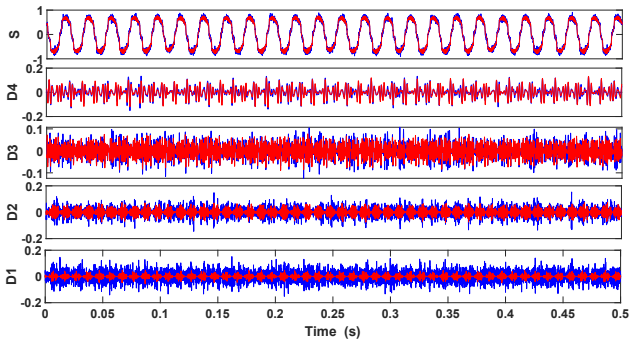

Fig. 14. The DWT of air gap magnetic field in a healthy case without noise impact (red), and with 20 dB SNR (blue).

TABLE III
THE ENERGY OF VARIOUS DWT SUB-BANDS APPLIED TO AIR-GAP MAGNETIC FIELD SIGNAL IN A HEALTHY AND UNDER ITSC FAULT.

	D6	***D5***	***D4***	***D3***	***D2***	***D1***
Healthy - No-Noise	0.83	0.94	0.97	1.0	1.06	1.35
Faulty - No-Noise	0.81	0.88	0.83	0.79	0.72	0.65
Healthy - 20 dB	0.81	0.88	0.83	0.79	0.72	0.65

reconstructed phase space using the dynamical system theory [26]. A single sampled state variable can generate a metrically equivalent state space, in addition, a dynamical invariant is also preserved in the reconstructed state space. If the trend of time variation of the signal is high, its average value for the different operating points may be utilized to extract a feature. The air-gap magnetic field signal is considered as a state variable to create the state space of the generator.

The reconstructed state space can be developed using time-delay embedding and derivative embedding approaches. The method based on derivative embedding includes higher-order derivates that make its application impractical in noisy environments indicating that time delay embedding is the proper approach for TSDM development. The invariant of the dynamical system in the time delay embedding method is found by transforming scalar points into a vector form [27]–[29].

For a given time series of the magnetic field of the air gap, as below:

$$B = \{B(k) - B(k-1)\} k = 2, 3, ..., j \tag{5}$$

where j is the number of the sampled signal, and k is the time index. The reconstructed phase space for k equal to 10 is shown in Fig. 15. A TDSM is used to generate the mass (gyration) based on variation in the magnetic field time series. The variation in a radius of gyration (RG) is a suitable tool for feature extraction from the air-gap magnetic field of a faulty machine. The RG is calculated from the generated mass to quantify the rate of changes due to ITSC fault, as follows [30]:

$$RG = \sqrt{\frac{\sum_{k=l+1}^{j} (B(k-\mu_0)^2 + (B(k-l)-\mu_l)^2}{j-l}} \tag{6}$$

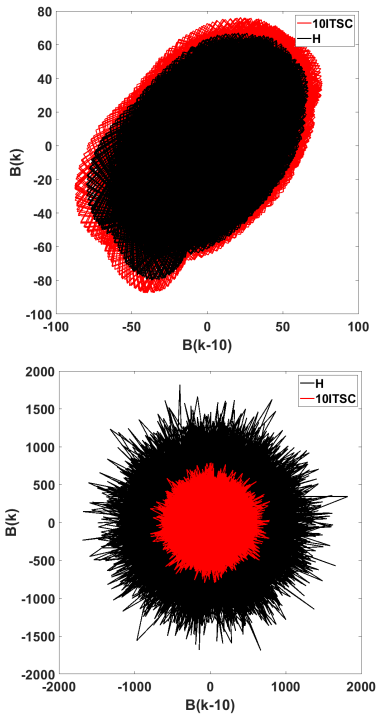

Fig. 15. The gyration radius of the air gap magnetic field in a healthy and a 10 ITSC fault without noise impact (top) and with a 20 dB SNR (bottom).

where μ_0 and μ_l are the center of gyration for their respective dimension, and l is the time lag of the phase space. The TSDM is able to point out the variation in the signal that is changed due to fault. However, the fault detection based on TSDM requires a priori knowledge of the healthy state of the machine for comparison. Although the processed signal by TSDM indicates the fault sign in the machine, the extracted feature is not informative to provide more insight into the fault type recognition.

As shown in Fig. 15, the fault leads to distortion of the magnetic field, which results in an increment in the radius of gyration. The calculated RG to magnetic flux density in the healthy state and under a 10 ITSC fault is 61 and 78, respectively. Fig. 15 represents the application of TSDM to the healthy and faulty air gap magnetic field in a presence of 20 dB white Gaussian noise. The magnitude of the RG is increased considerably compared with the signal without the noise effect. Moreover, the area of the mass and, correspondingly, the RG in healthy cases is enormously larger than in the faulty case. This results in false identification of a fault and indicates that the signal input to the TSDM algorithm must be noiseless, otherwise it leads to an inaccurate feature.

V. Hardware Noise Rejection

Every wire in the electrical instrument behaves like an antenna that absorbs the electromagnetic energy emitted from electrical equipment in the environment and converts it into an electrical signal with low amplitude. Therefore, rejecting this noise or reducing its impact on the measured signal is essential. A couple of simple solutions are shown below:

1) Grounding the machine frame diminishes the environmental noise effect.
2) Protecting a circuit or wires which are exposed to noise with a conducting material like a copper foil.
3) Reducing the length of wire used for data transmission or preferably using a coaxial cable.
4) Using the low-pass filter implemented in the measurement instrument.

Since the air-gap magnetic field measured in the laboratory is vulnerable to noise, copper foil is used to shield the sensor wires all the way to the DC power supply. The connection between the DC power supply to the oscilloscope is made with a coaxial cable. In addition, the SNR of the measured air-gap magnetic field is increased by increasing the magnitude of the current feeding into the Hall-effect sensor. The body of the generator is grounded in to avoid additional noise leaking into the sensor.

VI. Conclusion

This paper discussed thoroughly the various kinds of noise that may exist in the industrial environment and demonstrated how it can negatively affect the measured data. A detailed investigation of the frequency component of the measured noisy data in both laboratory and hydropower plants revealed that white Gaussian noise exists and is the most prevalent type of noise in power industries.

Signal processing tools are key to fault detection procedures for electrical machines. Based on the level of leaked noise into the signal, the processed data may indicate a false result. Indicating that noise must be measured in industry and power plants during data acquisition. Although, the main criteria to select a proper signal processing tool is its ability to track the fault frequency and performing algorithm in real-time with low computational burden, the level of noise must also be considered during the fault detection procedure. In order to show how signal processing tools work in a noisy environment, the air gap magnetic field of a 100 kVA salient pole synchronous generator in a healthy state and under ITSC fault is measured. The Hall-effect sensor is used to measure the air-gap magnetic field, since it is susceptible to the magnetic noise from inside the generator and noise from the working environment of the generator. Different signal processing tools, such as FFT, STFT, CWT, DWT, and TSDM, are used for ITSC fault detection. Suitable features were introduced and their performance in the presence of noise are evaluated and summarized below:

1) FFT: FFT can provide a general picture of the health state of the machine since it cannot reveal the fault type. Moreover, fault detection based on FFT requires a priori data of a healthy machine for comparison. FFT is only sensitive to high-level noise, and side-bands are masked if SNR is higher than 20 dB.
2) STFT: STFT can indicate the fault harmonics if a proper window function is selected and the parameters are adjusted precisely. The computational complexity of the STFT is n times a FFT, however, it can be used in real-time fault detection. Its sensitivity to noise and resolution of the frequency bands depends on the length

of the window and may result in a false alarm for SNR below 40 dB.

3) CWT: Application of CWT in fault detection provides a pattern that indicates the harmonics variation both in time and frequency. The selection of a proper mother wavelet is a key factor to track the fault harmonics. The computational complexity of the CWT compared with STFT and FFT is lower that makes its real-time implementation easier. CWT works fine with an SNR up to 40 dB, although its time-frequency plot becomes blurry. However, fault identification is still possible. CWT generates a chaotic representation of a signal with SNR above 40 dB and interpreting the plot is impossible.
4) DWT: Selection of a proper number of sub-bands plays a key role in precise fault harmonic track. A proper mathematical tool based on the signal property must be applied to the signal to indicate the effect of fault harmonic in the selected sub-band. The computational complexity of the DWT is similar to CWT. It depends on a frequency sub-band, which is utilized for feature extraction. If a feature is defined based on low-frequency sub-bands like D8 to D6, even a signal with SNR above 20 dB could not disturb the data.
5) TDSM: Although extracted feature based on variation in RG shows a fault harmonic impact on the measured signal, It is highly sensitive to noisy data, and it is not a useful tool if a signal is measured in a noisy environment.

REFERENCES

[1] H. Ehya, I. Sadeghi, and J. Faiz, "Online condition monitoring of large synchronous generator under eccentricity fault," in *2017 12th IEEE Conference on Industrial Electronics and Applications (ICIEA)*, 2017, pp. 19–24.

[2] P. Vijayraghavan and R. Krishnan, "Noise in electric machines: A review," *IEEE Transactions on Industry Applications*, vol. 35, no. 5, pp. 1007–1013, 1999.

[3] R. S. Girgis, M. Bernesjo, and J. Anger, "Comprehensive analysis of load noise of power transformers," in *2009 IEEE Power Energy Society General Meeting*, 2009, pp. 1–7.

[4] S. Yang, "Effects of voltage/current harmonics on noise emission from induction motors," in *Vibrations and Audible Noise in Alternating Current Machines*. Springer, 1988, pp. 457–468.

[5] H. Tischmacher, I. P. Tsoumas, B. Eichinger, and U. Werner, "Case studies of acoustic noise emission from inverter-fed asynchronous machines," *IEEE Transactions on Industry Applications*, vol. 47, no. 5, pp. 2013–2022, 2011.

[6] I. P. Tsoumas and H. Tischmacher, "Influence of the inverter's modulation technique on the audible noise of electric motors," *IEEE Transactions on Industry Applications*, vol. 50, no. 1, pp. 269–278, 2013.

[7] J. Qin, P. Sun, and J. Walker, "Measurement of field complex noise using a novel acoustic detection system," in *2014 IEEE AUTOTEST*. IEEE, 2014, pp. 177–182.

[8] S. M. J. Ali, "Measurement of vibration and noise level at power plant and refinery companies that represents a condition monitory for the health of machines," in *2017 International Conference on Environmental Impacts of the Oil and Gas Industries: Kurdistan Region of Iraq as a Case Study (EIOGI)*. IEEE, 2017, pp. 85–87.

[9] D. P. Martins and M. S. Alencar, "A new approach to noise measurement and analysis in an industrial facility," in *2014 IEEE International Instrumentation and Measurement Technology Conference (I2MTC) Proceedings*. IEEE, 2014, pp. 964–967.

[10] V. Ghorbanian and J. Faiz, "A survey on time and frequency characteristics of induction motors with broken rotor bars in line-start and inverter-fed modes," *Mechanical Systems and Signal Processing*, vol. 54-55, pp. 427 – 456, 2015. [Online]. Available: http://www.sciencedirect.com/science/article/pii/S0888327014003392

[11] J. Faiz and H. Nejadi-Koti, "Demagnetization fault indexes in permanent magnet synchronous motors—an overview," *IEEE Transactions on Magnetics*, vol. 52, no. 4, pp. 1–11, 2016.

[12] J. Faiz, H. Nejadi-Koti, and Z. Valipour, "Comprehensive review on inter-turn fault indexes in permanent magnet motors," *IET Electric Power Applications*, vol. 11, no. 1, pp. 142–156, 2017.

[13] M. Riera-Guasp, J. A. Antonino-Daviu, and G. Capolino, "Advances in electrical machine, power electronic, and drive condition monitoring and fault detection: State of the art," *IEEE Transactions on Industrial Electronics*, vol. 62, no. 3, pp. 1746–1759, 2015.

[14] I. Sadeghi, H. Ehya, J. Faiz, and A. A. S. Akmal, "Online condition monitoring of large synchronous generator under short circuit fault — a review," in *2018 IEEE International Conference on Industrial Technology (ICIT)*, 2018, pp. 1843–1848.

[15] J. Antonino-Daviu, V. Fuster-Roig, S. Park, Y. Park, H. Choi, J. Park, and S. B. Lee, "Electrical monitoring of damper bar condition in salient-pole synchronous motors without motor disassembly," *IEEE Transactions on Industry Applications*, vol. 56, no. 2, pp. 1423–1431, 2020.

[16] J. Yun, S. W. Park, C. Yang, S. B. Lee, J. A. Antonino-Daviu, M. Sasic, and G. C. Stone, "Airgap search coil-based detection of damper bar failures in salient pole synchronous motors," *IEEE Transactions on Industry Applications*, vol. 55, no. 4, pp. 3640–3648, 2019.

[17] Y. Park, S. B. Lee, J. Yun, M. Sasic, and G. C. Stone, "Air gap flux-based detection and classification of damper bar and field winding faults in salient pole synchronous motors," *IEEE Transactions on Industry Applications*, vol. 56, no. 4, pp. 3506–3515, 2020.

[18] G. Georgoulas, V. Climente, J. A. Antonino-Daviu, I. P. Tsoumas, C. D. Stylios, A. Arkkio, and G. Nikolakopoulos, "The use of a multilabel classification framework for the detection of broken bars and mixed eccentricity faults based on the start-up transient," *IEEE Transactions on Industrial Informatics*, vol. 13, no. 2, pp. 625–634, 2017.

[19] J. Pons-Llinares, J. A. Antonino-Daviu, M. Riera-Guasp, S. Bin Lee, T. Kang, and C. Yang, "Advanced induction motor rotor fault diagnosis via continuous and discrete time–frequency tools," *IEEE Transactions on Industrial Electronics*, vol. 62, no. 3, pp. 1791–1802, 2015.

[20] H. Ehya, A. Nysveen, R. Nilssen, and Y. Liu, "Static and dynamic eccentricity fault diagnosis of large salient pole synchronous generators by means of external magnetic field," *IET Electric Power Application*, vol. 34, no. 2, 2021.

[21] M. Heydarzadeh, M. Zafarani, M. Nourani, and B. Akin, "A wavelet-based fault diagnosis approach for permanent magnet synchronous motors," *IEEE Transactions on Energy Conversion*, vol. 34, no. 2, pp. 761–772, 2019.

[22] B. M. Ebrahimi, J. Faiz, and M. J. Roshtkhari, "Static-, dynamic-, and mixed-eccentricity fault diagnoses in permanent-magnet synchronous motors," *IEEE Transactions on Industrial Electronics*, vol. 56, no. 11, pp. 4727–4739, 2009.

[23] E. O. Brigham, *The fast Fourier transform and its applications*. Prentice-Hall, Inc., 1988.

[24] C. Torrence and G. P. Compo, "A practical guide to wavelet analysis," *Bulletin of the American Meteorological society*, vol. 79, no. 1, pp. 61–78, 1998.

[25] B. Lee *et al.*, "Application of the discrete wavelet transform to the monitoring of tool failure in end milling using the spindle motor current," *The International Journal of Advanced Manufacturing Technology*, vol. 15, no. 4, pp. 238–243, 1999.

[26] D. A. Rand and L.-S. Young, *Dynamical Systems and Turbulence, Warwick 1980: Proc. Symp. Held at the University of Warwick 1979/80*. Springer, 2006, vol. 898.

[27] H. Ehya, A. Nysveen, R. Nilssen, and U. Lundin, "Time domain signature analysis of synchronous generator under broken damper bar fault," in *IECON 2019 - 45th Annual Conference of the IEEE Industrial Electronics Society*, vol. 1, 2019, pp. 1423–1428.

[28] F. Takens, "Detecting strange attractors in turbulence," in *Dynamical systems and turbulence, Warwick 1980*. Springer, 1981, pp. 366–381.

[29] A. R. Webb, *Statistical pattern recognition*. John Wiley & Sons, 2003.

[30] R. J. Povinelli, J. F. Bangura, N. A. O. Demerdash, and R. H. Brown, "Diagnostics of bar and end-ring connector breakage faults in polyphase induction motors through a novel dual track of time-series data mining and time-stepping coupled fe-state space modeling," *IEEE Trans. Energy Convers*, vol. 17, no. 1, pp. 39–46, March 2002.